Binary Image Reconstruction from Two Projections and Skeletal Information

Norbert Hantos, Péter Balázs, Kálmán Palágyi

Department of Image Processing and Computer Graphics
University of Szeged
Árpád tér 2. H-6720, Szeged, Hungary
{nhantos,pbalazs,palagyi}@inf.u-szeged.hu

Abstract. In binary tomography, the goal is to reconstruct binary images from a small set of their projections. However, especially when only two projections are used, the task can be extremely underdetermined. In this paper, we show how to reduce ambiguity by using the morphological skeleton of the image as a priori. Three different variants of our method based on Simulated Annealing are tested using artificial binary images, and compared by reconstruction time and error.

Keywords: Binary tomography, Reconstruction, Morphological skeleton, Simulated annealing

1 Introduction

Binary tomography [7] aims to reconstruct binary images from their projections. In the most common applications of this field, e.g., electron tomography [1, 2] and non-destructive testing [3], usually just few projections of the object can be measured, since the acquisition of the projection data can be expensive or damage the object. Moreover, the physical limitations of the imaging devices make it sometimes impossible to take projections from numerous angles. Owing to the small number of projections the binary reconstruction can be extremely ambiguous. A common way to reduce the number of solutions of the reconstruction task is to assume that certain geometrical properties (e.g., convexity and/or connectedness) are satisfied.

In this paper we investigate a new kind of prior information, the skeleton of the image to be reconstructed. Skeleton is a region-based shape descriptor which represents the general form of binary objects [6]. One way of defining the skeleton of a 2-dimensional continuous object is as the set of the centers of all maximal inscribed (open) disks [5]. A disk is maximal inscribed if it is included in an object, but it is not contained by any other inscribed disk. The skeleton of a discrete binary image can be characterized via morphological operations [6], where disks are approximated by successive dilations of the selected structuring element that represents the unit disk. An interesting property of the morphological skeleton is that the original binary image can be exactly reconstructed from the skeletal subsets. In this work, we deal with the reconstruction problem

in which the entire morphological skeleton (instead of the individual skeletal subsets) and two projections of the original image are known.

In the reconstruction process the prior knowledge is often incorporated into an energy function, thus the reconstruction task is equivalent to a function minimization problem. There are various methods to solve that kind of problems [4, 9, 11]. In this paper, we show how to use Simulated Annealing (SA) for the binary reconstruction problem using two projections and the morphological skeleton. We show that, although theoretically the problem is non-unique, under some circumstances an acceptable image quality can be achieved. We propose three variants of a method to solve the above problem, based on parametric SA reconstruction.

The paper is structured as follows. In Section 2 we introduce the binary reconstruction problem, and show how to describe it as an energy minimization task. The morphological skeleton as an additional information to the reconstruction is presented in Section 3. In Section 4 we describe the problem of using skeletal information in the reconstruction and introduce the proposed algorithms to solve this task. In Section 5 we present experimental results and provide an explanation of them. Finally, we summarize our work and mention some of its possible extensions in Section 6.

2   The Two-Projection Binary Reconstruction Problem

In binary tomography the task is to reconstruct a two-dimensional binary image from a set of projections. The image can be represented by a binary matrix, and its *horizontal and vertical projection* can be defined as the vector of the row and column sums, respectively, of the image matrix. The task is now to reconstruct the binary image F from its horizontal and vertical projections, $\mathcal{H}(F)$ and $\mathcal{V}(F)$, respectively. Throughout this paper – without loss of generality – we assume square images of size $n \times n$.

The first method to solve the above problem was published in [10]. In the same work it was also showed that the solution is not always uniquely determined. Furthermore, in practical applications noisy projection data also complicates the reconstruction. A common way to overcome those problems is to transform the original task to a function minimization problem

$$f(\mathbf{x}) = ||\mathbf{A}\mathbf{x} - \mathbf{b}||_2^2 + \alpha \cdot g(\mathbf{x}) \quad \rightarrow \quad \min , \tag{1}$$

where $||.||_2$ stands for the Euclidean norm, $\mathbf{x}$ is an $n^2 \times 1$ binary vector representing the unknown image in a vector form using row-by-row traversal; $\mathbf{b} = \left(\mathcal{H}(F), \mathcal{V}(F)\right)^T$ is a $2n \times 1$ vector containing the projections and $\mathbf{A}$ is a $2n \times n^2$ binary matrix, where $a_{ij} = 1$ if and only if the pixel x_i is in relation with the j-th projection ray, 0 otherwise. The function $g(\mathbf{x})$ provides additional information, such as shape, connectivity, perimeter, etc. The lower value it takes the closer the reconstructed image to the expected one. It is multiplied by the weighting parameter $\alpha > 0$. In this paper we show how to use morphological skeleton as additional information.

3   Morphological Skeleton

The morphological skeleton $S(F, Y)$ of a discrete set of points $F \subset \mathbb{Z}^2$ determined by a structuring element $Y \subset \mathbb{Z}^2$ consists of the centers of all maximal inscribed discrete disks of radius k $(k = 0, 1, \ldots)$ [6]. With this approach, the structuring element Y is assumed to be the unit disk (i.e., a disk of radius 1) and the discrete disk Y^k of radius k is derived from Y by successive dilations:

$$Y^k = (\ldots (((\{\mathcal{O}\} \underbrace{\oplus Y) \oplus Y) \oplus \ldots) \oplus Y}_{k\text{-times}} \,, \tag{2}$$

where $\mathcal{O}$ and "$\oplus$" denote origin and the fundamental morphological operation called dilation [6], respectively.

The morphological skeleton $S(F, Y)$ is defined by

$$S(F, Y) = \bigcup_{k=0}^{K} S_k(F, Y) \; = \bigcup_{k=0}^{K} (F \ominus Y^k) - [(F \ominus Y^{k+1}) \oplus Y] \,, \tag{3}$$

where "$\ominus$" denotes the erosion (i.e., a morphological operation that is dual to dilation) [6], and K is the radius of the largest inscribed disk. In other words,

$$K = \max\{ \; k \mid F \ominus Y^k \neq \emptyset \; \}. \tag{4}$$

According to the formulation defined by Eq. 3, the morphological skeleton is the union of the disjoint skeletal subsets, where $S_k(F, Y)$ contains the centers of all maximal inscribed disks of radius k $(k = 0, 1, \ldots, K)$. An interesting property of the morphological skeleton is that a set F can be exactly reconstructed from the skeletal subsets:

$$F = \bigcup_{k=0}^{K} S_k(F, Y) \oplus Y^k \; = \bigcup_{p \in S(F, Y)} p \oplus Y^{k_p}, \tag{5}$$

where k_p is a unique value for each p such that $p \in S_{k_p}(F, Y)$.

From now we assume that structuring element Y corresponds to the 4-neighbors of the origin:

$$Y = \{ \; (-1, 0), (0, -1), (0, 0), (0, 1), (1, 0) \; \} \,. \tag{6}$$

Figure 1 shows an example of morphological skeleton by that Y.

4   Problem Setting and the Proposed Method

Let $H \in \mathbb{R}^n$ and $V \in \mathbb{R}^n$ be two vectors, and $S \subset \mathbb{Z}^2$ be a finite set of points. Our task is to reconstruct an image F for which $S(F, Y) = S$, and which (at least approximately) satisfies $\mathcal{H}(F) = H$ and $\mathcal{V}(F) = V$ (see Fig. 2). Unfortunately, the problem is underdetermined, as the following lemma states.
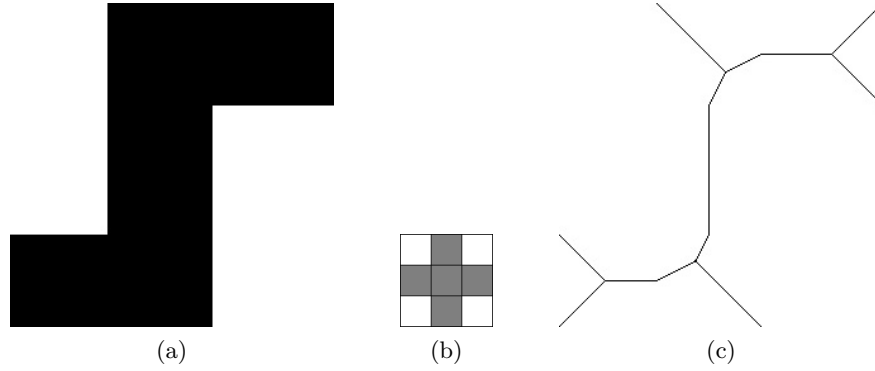
Fig. 1: Example of morphological skeleton. Original image F (a), the enlarged version of the considered structuring element Y (b), and the morphological skeleton $S(F,Y)$ (c).
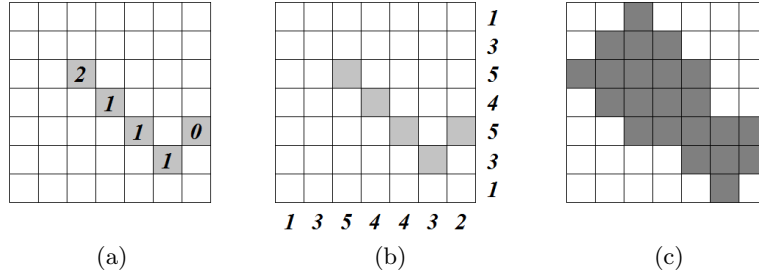

Fig. 2: Examples of two kinds of reconstruction problems. If k_p is known for each $p \in S(F,Y)$, F is uniquely reconstructable by Eq. 5 (a), the considered problem is to reconstruct F from $S(F,Y)$ and the two projections (b), image F to be reconstruced (c).

Lemma 1. *There may be some images with the same projections and morphological skeleton (i.e., the considered reconstruction problem is ambiguous).*

Proof. An example is given in Fig. 3. □

We know that for each point $p \in S(F,Y)$ there is a unique k_p value such that $p \in S_{k_p}(F,Y)$. Thus, the image F can be uniquely represented by a vector $K(S(F,Y)) = (k_{p_1}, k_{p_2}, \ldots, k_{p_{|S(F,Y)|}}) \in \mathbb{Z}^{|S(F,Y)|}$. Using the notions of Eq. 1 and given a set of points S, our goal is to find a $K^*(S) = (k_{p_1}^*, k_{p_2}^*, \ldots, k_{p_{|S|}}^*)$ which corresponds to the image F^* generated by Eq. 5, such that $f(\mathbf{x}^*) = ||\mathbf{A}\mathbf{x}^* - \mathbf{b}||_2^2$ is minimal. Here, $\mathbf{x}^*$ is the column vector representing F^*. Figure 4 shows an example. Note that even if there is no F such that $S = S(F,Y)$ and the function value of f is zero (e.g. in case of noisy data), it is still possible to give a solution, whose projections are close to the required ones.
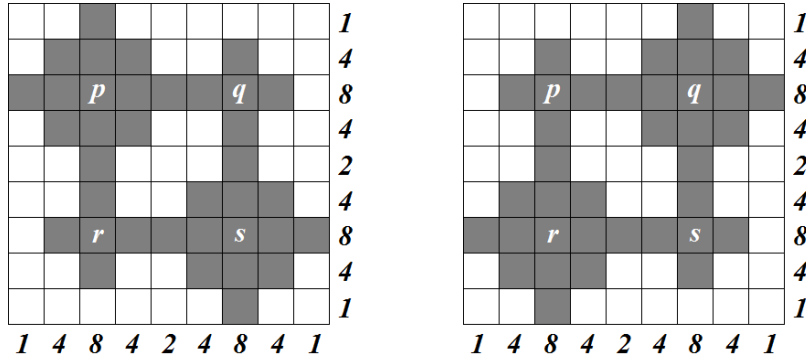
Fig. 3: Two different images F_1 and F_2 having the same projections and morphological skeleton, where $S(F_1, Y) = S(F_2, Y) = \{p, q, r, s\}$.
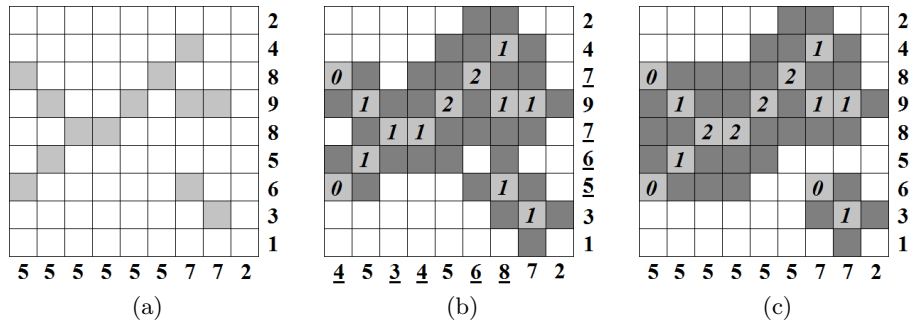

Fig. 4: Example of the studied reconstruction problem. The skeleton S and the required projections H and V (a), a possible solution F with $\mathcal{H}(F)$ and $\mathcal{V}(F)$ given by some $K(S)$ (b), the optimal solution F^* with $H = \mathcal{H}(F^*)$ and $V = \mathcal{V}(F^*)$ given by $K^*(S)$ (c). Projection elements that differ from the required ones are shown underlined.

The following lemma gives an upper bound for each element of $K(S(F, Y))$ of an arbitrary binary image F.

Lemma 2. *Let F be a binary image of size $n \times n$ and $K(S(F, Y)) = (k_{p_1}, k_{p_2}, \ldots, k_{p_{|S(F,Y)|}}) \in \mathbb{Z}^{|S(F,Y)|}$. Then $k_{p_i} \leq n/2$ for each $i = 1, \ldots, |S(F, Y)|$.*

Proof. From Eq. 4 we know that the maximum value of $K(S(F, Y))$ is $\max\{k \mid F \ominus Y^k \neq \emptyset\}$. Since the size of the structuring element Y is 3×3, it follows that $F \ominus Y^{n/2} = \emptyset$. Thus, the possible maximum value in $K(S(F, Y))$ is $n/2$. $\square$

Since the size of the image is known, the searching space is bounded by Lemma 2. The following lemma defines a sharper upper bound.

Lemma 3. *For any skeletal set of points S and for each $p = (i, j) \in S$ with the corresponding $k_{i,j} \in K(S)$*

$$k_{i,j} \leq \min \left\{ i - 1, \ j - 1, \ n - i, \ n - j, \ \frac{h_i}{2}, \ \frac{v_j}{2} \right\} \ ,$$

where h_i and v_j is the corresponding horizontal and vertical projection value, respectively.

Proof. It is trivial due to the size of the image and the size of $Y^{k_{i,j}}$. □

Lemma 2 and Lemma 3 define a unique maximum value for each $k_p \in K(S(F, Y))$. Additionally, we can use the following theorem for further reducing the searching space.

Theorem 1. *Let $S(F, Y)$ be the morphological skeleton of F generated with the structuring element Y defined by Eq. 6. Let $p, q \in S(F, Y)$, where $||p - q||_2 \leq \sqrt{2}$ (i.e., p and q are 8-adjacent to each other) and $p \in S_i(F)$, $q \in S_j(F)$ defined by Eq. 3. Then $|i - j| \leq 1$.*

Proof. Indirectly assume that $|i - j| > 1$, e.g., $i \geq j + 2$. We know from Eq. 3 that $q \in (F \ominus Y^j)$ but $q \notin (F \ominus Y^{j+1})$. Similarly $p \in (F \ominus Y^i)$. However, in that case $p \in (F \ominus Y^{j+2})$. Since p and q are 8-adjacent to each other, this also means that $q \in (F \ominus Y^{j+1})$, which is a contradiction. The case $j \geq i + 2$ can be seen analogously. □

Informally, if two skeletal points, p and q are 8-adjacent, then $|k_p - k_q| \leq 1$, if the structuring element is Y mentioned before. This can significantly reduce the searching space if the skeleton contains numerous pairs of 8-adjacent points.

There are numerous methods for solving Eq. 1. Since the function f is discrete and has many local minima, we propose to use Simulated Annealing (SA) [8]. Perhaps the most important advantage of the SA over the competitive methods is that it can guarantee a near optimal solution in a reasonable time. On the other hand, one serious drawback of the method is that one has to fine-tune many parameters to achieve an acceptable approximation of the global minimun of f. See Alg. 1 for the pseudo-code for SA.

The energy function f is simply $f(\mathbf{x}) = ||\mathbf{Ax} - \mathbf{b}||_2^2$, where $\mathbf{x}$ is defined by F. The goal is to find $K^*(S)$ which describe an image $\mathbf{x}^*$ where $f(\mathbf{x}^*)$ is minimal, i.e., it has the lowest energy. We know that if $f(\mathbf{x}_1) < f(\mathbf{x}_2)$, then the image F_1 is better than F_2 in the sense that its projections are closer to the required ones, therefore function $f(\mathbf{x})$ is a proper energy function. $T(t)$ is the temperature function or the cooling schedule, such that $T(0)$ is positive, and $T(t) \to 0$ as $t \to \infty$.

We choose the following exponential function

$$T(t) = T_0 \cdot \left(\frac{T_s}{T_0} \right)^{t/M} \ ,$$

Algorithm 1 Simulated Annealing on the Introduced Problem.

Input: projections H and V, set of skeletal points S and starting position $K_0(S)$
Output: $K(S)$
  $K(S) \leftarrow K_0(S)$
  $t \leftarrow 0$
  repeat
    $K'(S) \leftarrow \text{MODIFY}(K(S))$
    Calculate x' and x from $K'(S)$ and $K(S)$, respectively
    if $f(\mathbf{x}') < f(\mathbf{x})$ **or** $\text{RAND} < \exp\left(\frac{f(\mathbf{x}) - f(\mathbf{x}')}{T(t)} \right)$ **then**
      $K(S) \leftarrow K'(S)$
    end if
    $t \leftarrow t + 1$
  until the termination criterion is satisfied

---

where t denotes time, so the temperature will decrease over time, T_0 is the chosen value for the starting temperature and T_s is a technical parameter controlling the shape of the cooling schedule. We empirically established the starting temperature $T_0 = 10$ and the technical parameter $T_s = 0.001$. In each iteration step the time t is increased by 1. The process terminates when reaching M the maximal number of allowed iterations or zero energy.

RAND is a floating point number taken in each iteration from a uniform random distribution ($0 \leq \text{RAND} \leq 1$). With the function MODIFY we alter a state to another one simply by choosing a $k_p \in K(S)$ randomly and updating its value between the corresponding bounds. For the initial solution we choose the k_p-s such that the initial image satisfies Theorem 1 and its projections are close to the required ones. We developed three different strategies for the reconstruction:

1. *No Vase Constraint* (NVC): In the SA modification step, we choose a k_p randomly, and change it randomly between its bounds, omitting Theorem 1.
2. *Dynamic Vase Constraint* (DVC$_C$): We apply Theorem 1 in the following way: in each step, we modify a randomly chosen k_p by defining its new value such that $|k_p - k_q| \leq C$ holds for each q 8-adjacent to p. If $C = 1$, we allow only those differences that mentioned in Theorem 1. Because it also means slow convergence during iterations, we allow higher C values in the beginning of the reconstruction, and decrease C through time. For that we use a function $C(t)$, which is similar to the cooling schedule:

$$C(t) = \left\lceil C_0 \cdot \left(\frac{C_s}{C_0} \right)^{t/M} \right\rceil ,$$

where $\lceil . \rceil$ denotes the ceil function, C_0 is the starting parameter, so $C(0) = C_0$, C_s is a technical parameter established to 0.15 explicitly. Note that $C(t) \to 1$ as $t \to M$, so we force SA to search a solution that satisfies Theorem 1 as much as possible.

3. *Combined Energy Function* (CEF$_\alpha$): We incorporate the constraints of Theorem 1 by using an extended energy function:

$$f(\mathbf{x}) = \alpha||\mathbf{Ax} - \mathbf{b}||_2^2 + (1 - \alpha)g(\mathbf{x}),$$

where α is a weighting parameter ($0 \leq \alpha \leq 1$),

$$g(\mathbf{x}) = \sum_{||p-q||_2 \leq \sqrt{2}} h(k_p, k_q) \quad \big(p, q \in S, \ \ k_p, k_q \in K(S) \big),$$

and

$$h(k_p, k_q) = \begin{cases} 0 & \text{if } |k_p - k_q| \leq 1 \\ |k_p - k_q|/2 & \text{otherwise.} \end{cases}$$

Note that if a solution F satisfies Theorem 1, then $g(\mathbf{x}) = 0$. In case of $\alpha = 1$, this method is equivalent to the No Vase Constraint method (i.e. CEF$_1$ = NVC).

5   Results

5.1   Implementation Details

For testing our proposed methods we developed a general reconstruction framework. For initialization, one has to specify the initial temperature T_0, the technical parameter T_s, the maximal number of allowed iterations and the initialization method. Some of the solving methods could have additional parameters, such as α or C_0. Certain parameters were fixed, since they are not really relevant to the efficiency of the methods, such as C_s or the structuring element Y. We also fixed the cooling schedule, which is empirically established. The test was running under Windows 7 on an Intel Core 2 Duo T2520 of 1.5 GHz PC with 2GB of RAM.
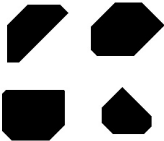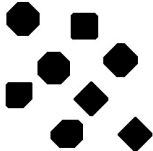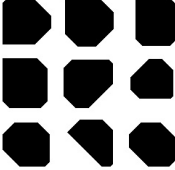
5.2   Experimental Results

We tested our algorithm on many images, in this paper we show eight samples of them. Six of our test samples have one point thin morphological skeleton consisting of few 8-connected components. However, we also show two other images which have more complex skeletons. All of the test images have the size of 256×256.

Since SA is a randomized algorithm, we performed each test 5 times and measured the mean CPU time and errors of the reconstruction. For the numerical evaluation of the quality of the reconstructed images, we calculated

$$E = ||\mathbf{b} - \mathbf{b}'||_2 \ ,$$

where $\mathbf{b}$ and $\mathbf{b}'$ are the projection vectors of the original and the reconstructed image, respectively For all tests, we set $T_0 = 10$, $T_s = 0.001$ and $M = 50\,000$.

Table 1: Reconstruction results. CPU values are in milliseconds and E values are rounded to integers. Best results are highlighted.

Image	Method	CPU	E	Image	Method	CPU	E
	NVC	3842	1060		NVC	7276	1285
	DVC_{10}	4030	98		DVC_{10}	7900	174
	DVC_5	4116	97		DVC_5	8127	146
	DVC_1	**4563**	**18**		**DVC_1**	**4473**	**0**
	$CEF_{0.3}$	4358	2468		$CEF_{0.3}$	7626	2578
	$CEF_{0.5}$	4415	1675		$CEF_{0.5}$	7665	1849
	$CEF_{0.7}$	4435	1305		$CEF_{0.7}$	7691	1505
	NVC	3784	3405		**NVC**	**4346**	**6136**
	DVC_{10}	**3038**	**1291**		DVC_{10}	4733	1066145
	DVC_5	3164	4288		DVC_5	4609	1722350
	DVC_1	3566	5307		DVC_1	4926	3302481
	$CEF_{0.3}$	5412	5665		$CEF_{0.3}$	7308	14371
	$CEF_{0.5}$	5387	4829		$CEF_{0.5}$	7243	8896
	$CEF_{0.7}$	5328	3212		$CEF_{0.7}$	7222	7402
	NVC	1666	1341		**NVC**	**2165**	**2709**
	DVC_{10}	**1215**	**292**		DVC_{10}	1713	6042
	DVC_5	1234	314		DVC_5	1724	7962
	DVC_1	1302	294		DVC_1	1910	6360
	$CEF_{0.3}$	2904	2534		$CEF_{0.3}$	4123	5688
	$CEF_{0.5}$	2827	1950		$CEF_{0.5}$	4131	4178
	$CEF_{0.7}$	2851	1732		$CEF_{0.7}$	4114	3346
	NVC	**3537**	**2530**		**NVC**	**2757**	**4034**
	DVC_{10}	2852	9154		DVC_{10}	2304	4523
	DVC_5	2981	13138		DVC_5	2467	7472
	DVC_1	3226	67493		DVC_1	2430	13096
	$CEF_{0.3}$	6380	5183		$CEF_{0.3}$	8884	6663
	$CEF_{0.5}$	6367	4102		$CEF_{0.5}$	8856	5012
	$CEF_{0.7}$	6343	3029		$CEF_{0.7}$	8959	4407

(a)   (b)   (c)
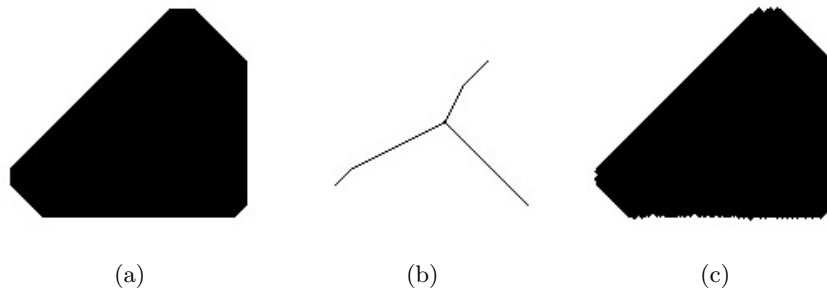
Fig. 5: A test image (a), its morphological skeleton (b), one of the reconstructed images with $CEF_{0.5}$ (c).

First, we tested the images containing just one convex object (see the first row of Table 1). An example for the reconstruction is shown in Fig. 5. We found that the results were mostly smooth enough, and 50 000 iterations were more than enough to converge to such a reconstructed image. All three methods provided good results, and DVC turned out to be the best choice. In one case, with certain parameters we could even perfectly reconstruct the original image in all 5 runs, using only 21 220 iterations on average.

In the second turn we studied the images of convex objects arranged in a 2×2 and a 3×3 array (second row of Table 1). We observed that the initial state misleaded the DVC algorithm in one of the images. The main reason is that the initial image is very dissimilar to the original one, and DVC converges very slowly.

The third group of test data contained images consisting of convex objects forming random groups (third row of Table 1). For the first image, the results are similar to the first group's results, even if there are more skeletal points now which yields a bigger searching space. However, for the second image NVC produced the best results.

Finally, we examined some images that have many skeletal points with few connections (fourth row of Table 1). An example reconstruction result can be seen in Fig. 6. One of the reasons for the poor results could be the skeleton, which contains many isolated pixels. It makes the method slow and ambiguous due to the large searching space. Here, NVC proved to be the best choice, since it does not use Theorem 1, yielding the most robust approach of all. Although even this method could reach just a rough approximation of the original object, the result is quite promising – regarding that just two projections were used.
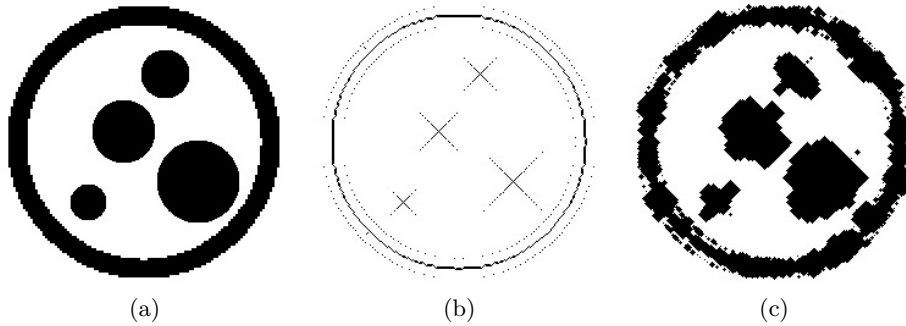

(a)   (b)   (c)

Fig. 6: A test image (a), its morphological skeleton that contains numerous isolated pixels (b), and one of the reconstructed images with NVC (c).

6   Conclusions and Further Work

We proposed three variants of a method based on Simulated Annealing to reconstruct binary images from their horizontal and vertical projections and their morphological skeleton. Without assuming 8-connected morphological skeletons, a rough reconstruction is always possible in a short time and a small number of iterations. With additional restrictions the result will be smoother, however, the convergency of the method becomes slower. The No Vase Constraint method provides overall satisfactory results, however, the Dynamic Vase Constraint creates smoother results in most cases, but needs more iterations to converge. The Combined Energy Function method is just slightly worse than the first method, but much slower. Beside that, in all the three considered methods we found that the result is much more dependent on the number of the skeletal points, rather than on the size of the image.

This paper is just an introduction of a novel approach and there are many open questions in the field. Since SA is rather sensitive to the initial state, in a further work, we want to apply further strategies for choosing a starting image, e.g., by using Ryser's algorithm to obtain an initial solution. Beside that, we try to find a more sophisticated function minimizer, or redefine our energy function in a way that it could be managed with deterministic mathematical tools – however, this seems to be a hard task. We assume that the problem is NP-hard. We also plan to examine the efficiency of the methods using more projections and other prior information, such as smoothness on the boundary. Finally, we also intend to study the robustness of the reconstruction when the projections are corrupted by noise.

Acknowledgements

References

1. Aert, S.V., Batenburg, K.J., Rossell, M.D., Erni, R., Tendeloo, G.V.: Three-dimensional atomic imaging of crystalline nanoparticles. Nature 470, 374-377 (2011)
2. Batenburg, K.J., Bals, S., Sijbers, J., Kuebel, C., Midgley, P.A., Hernandez, J.C., Kaiser, U., Encina, E.R., Coronado, E.A., Tendeloo, G.V.: 3D imaging of nanomaterials by discrete tomography. Ultramicroscopy 109(6), 730-740 (2009)
3. Baumann, J., Kiss, Z., Krimmel, S., Kuba, A., Nagy, A., Rodek, L., Schillinger, B., Stephan, J.: Discrete tomography methods for nondestructive testing. In: Herman,

G.T., Kuba, A. (Eds.) Advances in Discrete Tomography and Its Applications, pp. 303-331, Birkhäuser, Boston (2007)

4. Gesù, V.D., Bosco, G.L., Millonzi, F., Valenti, C.: A memetic algorithm for binary image reconstruction. In: Brimkov, V.E., Barneva, R.P., Hauptman, H.A. (Eds.) IWCIA 2008. LNCS, Vol. 4958, pp. 384-395. Springer, Heidelberg (2008)

5. Giblin, P., Kimia, B.B.: A formal classification of 3D medial axis points and their local geometry. IEEE Trans. Pattern Analysis and Machine Intelligence 26(2), 238-251 (2004)

6. Gonzalez, R.C., Woods, R.E.: Digital Image Processing (3rd Edition). Prentice Hall (2008)

7. Herman, G.T., Kuba, A. (Eds.): Advances in Discrete Tomography and Its Applications. Birkhäuser, Boston (2007)

8. Kirkpatrick, S., Gelatt Jr., C.D., Vecchi, M.P.: Optimization by Simulated Annealing. Science 220, 671-680 (1983)

9. Nagy, A., Kuba, A.: Parameter settings for reconstructing binary matrices from fan-beam projections. Journal of Computing and Information Technology 14(2), 100-110 (2006)

10. Ryser, H.J.: Combinatorial properties of matrices of zeros and ones. Canad. J. Math. 9, 371-377 (1957)

11. Schüle, T., Schnörr, C., Weber, S., Hornegger, J.: Discrete tomography by convex-concave regularization and D.C. programming. Discrete Applied Mathematics 151, 229-243 (2005)